

# Sedimentary response of a structural estuary to Holocene coseismic subsidence

Laura C. Reynolds<sup>1,5,†</sup>, Alexander R. Simms<sup>1</sup>, Thomas K. Rockwell<sup>2</sup>, Yusuke Yokoyama<sup>3</sup>, Yosuke Miyairi<sup>3</sup>, and Alexandra Hangsterfer<sup>4</sup>

<sup>1</sup>Department of Earth Science, 1006 Webb Hall, University of California, Santa Barbara, California 93106, USA

<sup>2</sup>Department of Geological Sciences, MC-1020, 5500 Campanile Dr., San Diego State University, San Diego, California 92182-1020, USA

<sup>3</sup>Atmosphere and Ocean Research Institute, The University of Tokyo, 5-1-5, Kashiwanoha, Kashiwa-shi, Chiba 277-8564, Japan

<sup>4</sup>Scripps Institution of Oceanography, 9500 Gilman Drive, La Jolla, California 92093, USA

<sup>5</sup>Department of Earth, Environment, and Physics, Worcester State University, 486 Chandler St., Worcester, Massachusetts 01602, USA

## ABSTRACT

Stratigraphic evidence for coseismic subsidence has been documented in active-margin estuaries throughout the world. Most of these studies have been conducted in subduction zone or strike-slip settings; however, the stratigraphic response to coseismic subsidence in other tectonic settings would benefit from further study. Here we show evidence of late Holocene coseismic subsidence in a structural estuary in southern California. Below the modern marsh surface, an organic-rich mud containing marsh gastropods, foraminifera, and geochemical signatures indicative of terrestrial influence (mud facies) is sharply overlain by a blue-gray sand containing intertidal and subtidal bivalves and geochemical signatures of marine influence (gray sand facies). We use well-established criteria to interpret this contact as representing an abrupt  $1.3 \pm 1.1$  m rise in relative sea level (RSL) generated by coseismic subsidence with some contribution from sediment compaction and/or erosion. The contact dates to  $1.0 \pm 0.3$  ka and is the only event indicative of rapid RSL rise in the 7 k.y. sedimentary record studied. Consistent with observations made in previous coseismic subsidence studies, an acceleration in tidal-flat sedimentation followed this abrupt increase in accommodation; however, the recovery of the estuary to its pre-subsidence elevations was spatially variable and required 500–900 years, which is longer than the recovery time estimated for estuaries with larger tidal ranges and wetter climates.

## INTRODUCTION

Evidence for individual coseismic subsidence events has been extensively demonstrated in tectonically active coastal regions throughout the world by the presence of marsh surfaces buried by intertidal sediments due to deformation from subduction zone earthquakes (Atwater, 1987; Atwater and Hemphill-Haley, 1997; Atwater et al., 2001; Hawkes et al., 2011; Reinhardt et al., 2010) and strike-slip earthquakes (Clark et al., 2013; Cochran et al., 2017; Knudsen et al., 2002). Localized coseismic subsidence related to movement along upper crustal structures has also been inferred for a variety of tectonic regimes (Bourgeois and Johnson, 2001; Cundy et al., 2000; McNeill et al., 1999; Pratt et al., 2015; Sherrod, 2001) and is the likely cause of subsidence documented in fault-bounded, structurally controlled estuaries outside the direct influence of subduction or strike-slip earthquakes (Cundy et al., 2000; Simms et al., 2016). Determining recurrence and magnitudes of coseismic subsidence is necessary to assess seismic hazards and can elucidate subsurface relationships among structures in complex tectonic regions (i.e., Shennan et al., 2016). However, differentiating the effects of coseismic subsidence from nonseismic processes that produce similar stratigraphic changes, such as floods, global mean sea-level rise, sediment flux-driven transgressions, local morphological changes (barrier breaching, mouth migration), or anthropogenic-induced subsidence, is difficult (Shennan et al., 2016), especially where subsidence is localized (i.e., within a structural estuary) rather than regional (i.e., megathrust-related crustal deformation).

Previous studies (Nelson et al., 1996, 1998; Shennan et al., 2016) have developed criteria for recognizing coseismic subsidence in the strati-

graphic record that are based mainly on observations from subduction zone earthquakes. These criteria include, but are not limited to, the following: a laterally extensive and sharp contact, evidence for a sudden relative sea level (RSL) rise, and evidence for synchronicity of change that is replicated in multiple cores. These characteristics are interpreted to represent the estuarine response to a sudden decrease in elevation (a rise in RSL).

While identification of subsidence in the sedimentary record is important for hazard assessment, it is also important to understand the completeness and limitations of estuarine sediments as recorders of seismic events (Atwater et al., 2001; Dura et al., 2016). Previous work has shown that the tidal range (Atwater et al., 2001), sediment supply and source (Darienzo and Peterson, 1990), and patterns of relative sea-level change (Dura et al., 2016) all influence the response of estuarine environments to vertical displacement and therefore their ability to stratigraphically record coseismic events. However, the variability in estuarine response to coseismic subsidence within these different contexts, i.e., how this variability is characterized in the stratigraphic record, has received relatively little attention.

Here we use sediment cores and relative sea-level indicators from Carpinteria Marsh, a small structural estuary in southern California, and show stratigraphic evidence for an abrupt environmental change that emplaced blue-gray sands on top of organic-rich, fine-grained muds throughout the marsh. We hypothesize that the contact represents an abrupt rise in RSL caused by coseismic subsidence along a local thrust fault. Using multi-proxy sea level indicators and a robust chronology, we test whether the nature of this contact is consistent with the criteria

Laura C. Reynolds  <https://orcid.org/0000-0001-7828-4662>

<sup>†</sup>laura.conners.reynolds@gmail.com.

developed to identify coseismic subsidence in the stratigraphic record and discuss its potential hazard and structural implications. We show that traditional criteria used to identify coseismic deformation events remain applicable for recognizing coseismic subsidence even when the subsidence appears to be highly localized within a structural estuary; however, the non-tectonic characteristics of the environment (tidal

range, sediment supply, and climatic context) must be carefully considered to differentiate coseismic events from other processes in these dynamic systems.

**STUDY AREA**

The study area, Carpinteria Marsh (34°24'N, 119°31'30"W), is located along the Santa Bar-

bara Channel in southern California, USA. The marsh lies within the axis of the Carpinteria basin, a small, faulted syncline (Jackson and Yeats, 1982; Fig. 1C) on the down-thrown side of the south-dipping, out-of-syncline (Mitra, 2002) Rincon Creek Fault (Jackson and Yeats, 1982). Carpinteria basin lies on the southern flank of the Santa Ynez Mountains (Fig. 1), which are part of the Western Transverse

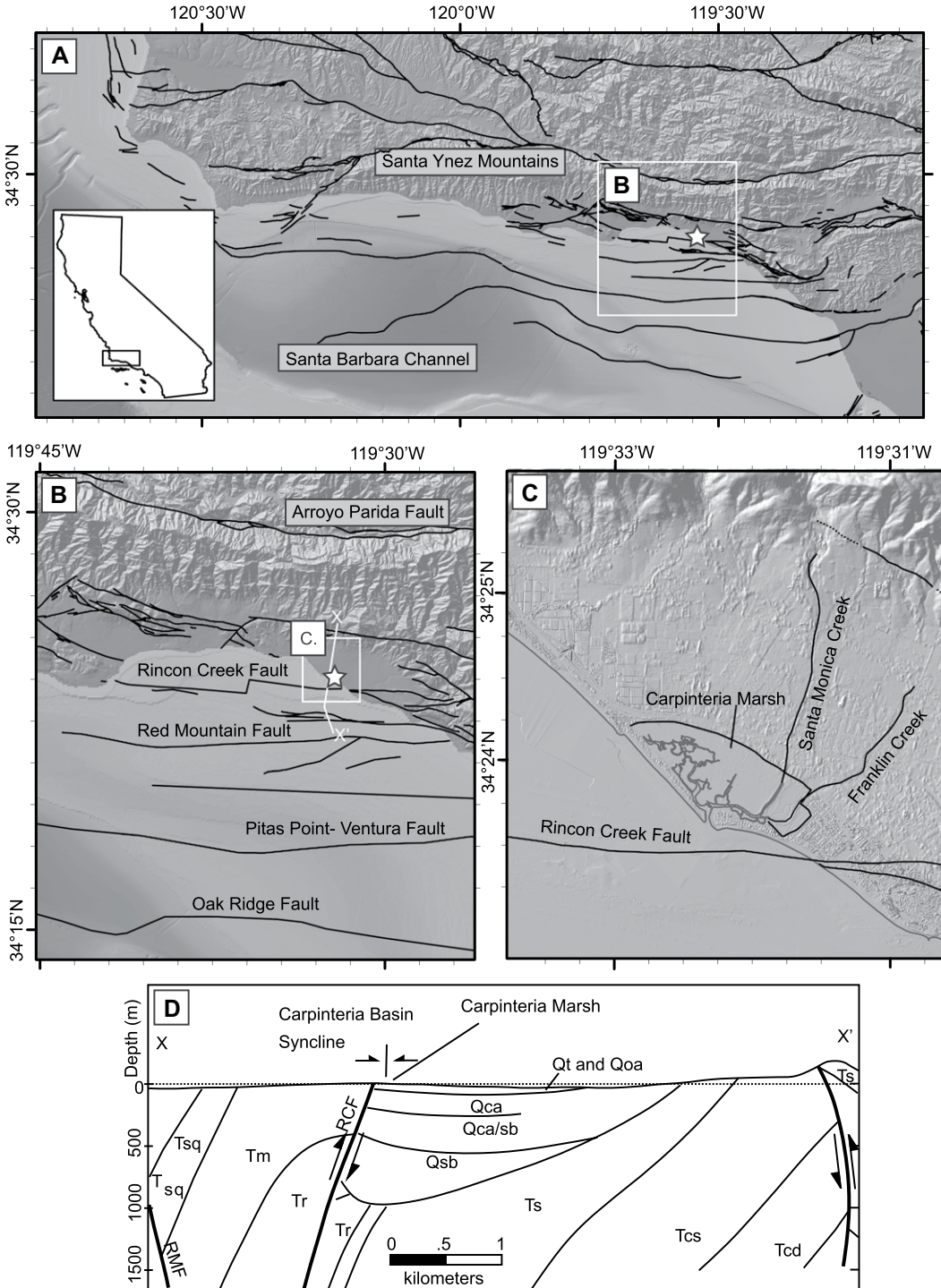


Figure 1. Location of Carpinteria Marsh is shown at three different scales in Panels A, B, and C. Locations noted in manuscript, including major Quaternary faults are shown (USGS, 2020). Carpinteria Marsh, the study site, is indicated by the white star in Panels A and B. The white line shows the location of the cross section. The cross section in the bottom panel (D) is adapted from Jackson and Yeats (1982) and Simms (2016).

Ranges, a large east-west–trending fold and thrust belt that has exhibited rapid uplift since the Pliocene resulting from compression due to a restraining bend in the San Andreas fault system (Jackson and Yeats, 1982; Rockwell et al., 2016). Large, north-dipping thrust faults in Ventura and Santa Barbara Counties, such as the Pitas Point–Ventura Fault (Fig. 1), may have the potential for Mw 7.5–8 earthquakes (Levy et al., 2019; Rockwell et al., 2016). However, the subsurface geometry, and therefore the extent of the regional seismic hazard, in the Ventura region is subject to ongoing debate (Hubbard et al., 2014; Jackson and Yeats, 1982; Johnson et al., 2017; Levy et al., 2019; Marshall et al., 2017; Rockwell et al., 2016); therefore, additional sedimentary records of seismic activity in the region may help clarify these interpretations.

Carpinteria Marsh is a fragment of a once larger estuary that prehistorically occupied much of the low-lying coastal plain of the Carpinteria basin (Ferren, 1985). The marsh is dominated by *Salicornia virginica*, marsh pickleweed (Hubbard, 1996; Page, 1995; Sadro et al., 2007), and receives tidal flow through an inlet stabilized with a rock revetment in 1964 (Ferren, 1985) and freshwater input from two tidal creeks (Santa Monica and Franklin Creeks) that enter the marsh's northeastern corner. The marsh has a tidal range of 1.01 m (Sadro et al., 2007), with high tide levels similar to those of the open coast, but truncated low water levels due to a lagged ebb tide from inlet constriction (Hubbard, 1996). Similar to observations in other salt marshes in California (i.e., Thorne et al., 2018), the vegetated marsh platform and mudflats range from mean low water (MLW) to elevations above mean higher high water (MHHW). The marsh is located in a Mediterranean climate region characterized by mild, wet winters and warm, dry summers (Bakker and Slack, 1984); most of the small streams that run from the mountains to the coast only flow and transport sediments during storm events. Historically, three to five freshwater streams built alluvial fans into the fringes of the marsh during storm events, but today the two remaining streams are channelized upstream from the marsh. One historical alluvial fan, attributed to a flood in 1914, is still visible in the northeastern corner of the marsh (Fig. 2; Ferren, 1985).

## METHODS

From 2012 to 2018, we collected 44 vibracores that sampled from 1 m to 4 m below ground surface and five Geoprobe 7822DT cores that sampled up to 14 m below ground surface in

Carpinteria Marsh (Fig. 1 and Supplemental Figs. S1–S3<sup>1</sup>) and established sedimentary facies using grain size, color, sedimentary structures, organic content, and foraminifera and shell taxonomy (Table 1). Core locations were determined with a TopCon Hyperlite + differential global positioning system (GPS) or a handheld GPS; core-top elevations were determined with the differential GPS or Lidar corrected for vegetation error (Sadro et al., 2007). Elevations were corrected to NAVD88 using the National Oceanic and Atmospheric Administration (NOAA) Online Positioning User Service site ([www.ngs.noaa.gov/OPUS/elevations](http://www.ngs.noaa.gov/OPUS/elevations); accessed September 2021). The vertical uncertainty for the ground surface elevation of all cores is less than 0.15 m. Sixty-eight organic, charcoal, and shell samples were used for radiocarbon analysis at the University of California Irvine Keck Carbon Cycle Accelerator Mass Spectrometer Laboratory, while 26 samples were analyzed at the Atmospheric and Ocean Research Institute (AORI) at The University of Tokyo (Yokoyama et al., 2010; Table S2; see footnote 1).

Thirty modern sediment samples collected from a transect along the marsh surface (see Supplemental Material 1 and Fig. S4; see footnote 1) and 175 sediment samples from core CM46 were freeze-dried, crushed, and treated with 3 N HCl at 100 °C to remove inorganic carbon in preparation for carbon isotope analyses. A Delta V Advantage and Flash 2000 Elemental Analyzer–Isotopic Ratio Mass Spectrometer (EA–IRMS) at AORI was used for isotopic analysis. Data were corrected for machine drift and amount-dependent deviations when necessary. Repeated analyses of internal standards indicated a  $2\sigma$  uncertainty of 0.86‰. Core CM46 was scanned at 0.2 mm resolution on an Avaatech X-Ray Fluorescence (XRF) core-scanner at Scripps Institution of Oceanography at 10 keV, 30 keV, and 50 keV, which measured a suite of 29 elements. X-ray spectra were processed following Addison et al. (2013), and log ratios of elemental counts were used in interpretations because log ratios are less affected by variations in the physical characteristics of sediments (water content, grain size, etc.) (Addison et al., 2013; Weltje and Tjallingii, 2008).

<sup>1</sup>Supplemental Material. Supplemental Materials 1 (supplemental figures S1, S2, S3, S4); Supplemental Materials 2 (Table S1. Core Information); Supplemental Materials 3 (Bacon and OxCal Scripts); and Supplemental Materials 4 (Invertebrate depth references). Please visit <https://doi.org/10.1130/GSAB.S.16834096> to access the supplemental material, and contact [editing@geosociety.org](mailto:editing@geosociety.org) with any questions.

## RESULTS

### Facies Descriptions and Interpretations

We follow Reynolds et al. (2018) in their designation of four sedimentary facies present in Carpinteria Marsh: gray sand facies, brown sand facies, mud facies, and white sand facies. These facies are described in detail in Reynolds et al. (2018), but we summarize their characteristics here as well as in Table 1. Deposits of white sand facies are localized to the upper meter of sediments throughout Carpinteria Marsh and were previously interpreted to represent a historical washover event (Reynolds et al., 2018); therefore, we do not discuss this facies further in this paper.

The gray sand facies is shell rich, gray in color, fine- to medium-grained sand with silt-sand laminations that are likely indicative of tidal influence, and it is often massive or mottled. Gray sand facies deposits are devoid of foraminifera and ostracods, similar to modern beach and dune sands in Carpinteria (Wilson et al., 2014). However, the gray sand facies deposits contain articulated and fragmented shells of intertidal and subtidal bivalves (*Mascoma nasuta*, *Chione undulata*, *Leukoma staminea*, *Tagelus californianus*, *Saxidomus nuttalli*, *Ostrea* spp., *Leukoma laciniata*, *Cryptomya californica*). Therefore, we interpret the gray sand facies to represent a lower intertidal to subtidal depositional environment.

The mud facies is characterized by fine-grained, organic-rich, laminated and bioturbated mud and silt deposits. Mud facies deposits contain foraminifera species that are indicative of a marsh environment (*Miliammina fusca*, *Trochammina inflata*, *Elphidium excavatum*, *Jadammina macrescens* (Avnaim-Katav et al., 2017; Bentz, 2016; Scott et al., 2011) and shells of *Cerithidea californica*, which is a mudflat/marsh gastropod (Sousa, 1983). This invertebrate assemblage is consistent with an intertidal mudflat/marsh environment.

The brown sand facies is characterized by fine- to coarse-grained sand beds, which are massive or normally graded. Beds of this facies often have sharp or erosional bases and contain ripple cross laminations or parallel laminations. The deposits are lithic-rich, brown in color, and are more common and thicker in the landward portions of the marsh. They lack shell material except for the occasional *C. californica* fragment. We interpret the brown sand facies to represent storm-derived flood deposits transported from the small streams draining into the marsh into an alluvial fan depositional environment at intertidal to supratidal elevations.



**Figure 2.** Locations of geoprobe cores and vibracores collected in this study, and approximate locations of cone penetration test (CPT) boreholes from previous research (Fugro West, 2004) in Carpinteria Marsh are shown. The top panel shows Carpinteria in 1929 and the bottom panel in 2007. Cores with gray sand facies are shown as black dots; cores that do not sample gray sand facies are shown as white dots. CPTs are shown as triangles. Cross sections illustrated in Figure 3 are shown as white lines. In both images, the alluvial fan attributed to a flood in 1914 (Ferren, 1985) is clearly visible in the marsh's northeast corner, outlined by the white dashed line.

### Stratigraphy and Evidence for Environmental Change

At the base of all cores that penetrate below 10 m, NAVD88 is a bed of gray sand facies, which grades upwards into beds of mud facies

that are interbedded with beds of brown sand facies (Fig. 3; Simms et al., 2016). At ~2–3.5 m NAVD88, the mud facies and brown sand facies deposits are sharply overlain by a bed of gray sand facies except in six cores around the landward perimeter of the marsh, in which deposits of

gray sand facies are absent at the depths sampled (Fig. 2). The contact between deposits of mud facies and the overlying gray sand facies, hereafter referred to simply as “the contact” (Fig. 3), is directly sampled in seven cores and represents a distinct lithostratigraphic, geochemical, and

TABLE 1. FACIES DESCRIPTIONS, INTERPRETATIONS, AND INDICATIVE RANGES

Facies (Reynolds et al., 2018)	Facies description	Facies interpretation	Indicative range	Indicative range (modern values, relative to NAVD88) (m)
Mud facies	Organic-rich; fine-grained (clay to fine sand, mean grain size <50 $\mu\text{m}$ ); massive, mottled, or laminated; colors range from blue-grey to red-brown; whole and partial <i>Cerithidea californica</i> shells are common, other shell fragments rare; sparse marsh and mudflat foraminifera include <i>Jadammina macrescens</i> , <i>Milliammina fusca</i> , <i>Elphidium</i> spp., <i>Ammonia</i> spp., and <i>Trochiammina</i> spp.; beds range from a few centimeters to 1 m thick; interbedded with brown sand facies	Marsh and mudflats	MLW* to HAT <sup>†</sup>	0.70–2.16
Grey sand facies	Generally organic-poor with some small (millimeter-scale) plant fragments; fine- to medium-grained sand (mean grain size 50–150 $\mu\text{m}$ ); light to dark grey in color; poorly sorted with few muddy silt lamina that are frequently mottled or faintly laminated; abundant shells and shell fragments include <i>Ostrea</i> spp., <i>Saxidomus nuttalli</i> , <i>Macoma nasuta</i> , <i>Leukoma laciniata</i> ; devoid of foraminifera; beds are meter-scale in thickness; grade into or are sharply overlain by beds of mud facies or brown sand facies	Low intertidal or subtidal sand flats and/or lagoon	LAT <sup>†</sup> to MSL*	–0.66–1.02
Brown sand facies	Organic-poor; sandy silt to medium-grained sand (mean grain size 20–112 $\mu\text{m}$ ); brown colored; poorly sorted, scattered granules, laminated, massive and normally graded beds; no shells or shell fragments or foraminifera; beds 1–50 cm thick; interbedded with mud facies and most common in the cores at the landward edges of the marsh	Alluvial fan (flood) deposits	> MLW*	>0.70

\*Mean low water (MLW), mean sea level (MSL) modern values are from Sadro et al. (2007).  
<sup>†</sup>Lowest, highest astronomical tide (LAT, HAT) modern values are from National Oceanic and Atmospheric Administration (Santa Barbara Station NOAA tide gauge [<http://tidesandcurrents.noaa.gov>]).

biological boundary. It is interpreted to represent an abrupt environmental change from a marsh environment (as indicated by mud facies deposits) to a relatively lower elevation estuarine/lagoon environmental (as indicated by gray sand facies deposits). The contact itself is sharp (<1 mm) or irregular, which indicates nondeposition or erosion. The gray sand facies deposits above the contact often contain muddy rip up clasts, which indicate that the contact represents a high energy, erosive event.

While both the XRF and  $\delta^{13}\text{C}$  data are highly variable, their general patterns are consistent with interpretations of an abrupt environmental change at the contact that emplaced relatively lower elevation gray sand facies deposits on higher elevation mud facies deposits. The mud below the contact has low Sr/Ti and Ca/Ti and high Fe/Ti ratios, but this pattern abruptly reverses above the contact. Sr and Ca ratios have been qualitatively associated with increased salinity (Koutsodendris et al., 2017), although they can also indicate the presence of freshwater carbonate (Chague-Goff et al., 2017). Therefore, we suggest the increase in Sr and Ca above the contact may indicate an increase in marine influence relative to the sediments below the contact, but additional research (calibrations or identification of marine diatoms, for example) would be needed to confirm this interpretation. In addition, the bulk sediment  $\delta^{13}\text{C}$  values gradually increase above the contact, which potentially reflects an increase in marine carbon input, as has been interpreted in other studies (Milker et al., 2015). The gradual nature of this change and the variability in  $\delta^{13}\text{C}$  values within gray sand facies deposits likely reflect the mixed sources of carbon present, which would include both marine-

derived carbon as well as carbon redeposited from estuarine sources (within rip ups, etc.).

Above the contact, the nature of the gray sand facies is highly variable, and individual beds of sand are difficult to correlate spatially. Deposits of gray sand facies grade upwards into the top-most sediments in the marsh, which are comprised of beds of mud facies interbedded with beds of brown sand facies (Fig. 3; Reynolds et al., 2018). We interpret this transition to represent the gradual shoaling of the estuary to its previous elevations and the marsh/mudflat environment that characterizes the marsh today.

The core stratigraphy suggests the contact is correlative throughout the marsh where gray sand facies deposits are found. In addition, a geotechnical survey from 2004 (Fugro West, 2004) includes cone penetration test (CPT) and borehole data from the eastern side of the marsh, which were interpreted to reflect grain size changes in the subsurface. The inferred grain size patterns indicate a contact between generally finer grained deposits and overlying sand deposits (described in the report as gray or brown estuarine sand where sampled) at similar elevations to those of the contact we observe, which indicates that the contact may extend at least along the entire shore-parallel length of the marsh and as far landward as Carpinteria Avenue (Fig. 1).

### Quantifying the Magnitude of RSL Change

The lithological and biological evidence presented above indicates that the contact marks a deepening of the estuary from a higher elevation (intertidal) mudflat/marsh environment characterized by fine-grained sediment deposition of

mud facies sediments to a lower elevation (subtidal to intertidal), tidally influenced sand flat or shallow lagoon environment in which gray sand facies sediments were deposited. To estimate the magnitude of the inferred deepening, we estimated the indicative meaning (i.e., the vertical relationship to a reference water level; Shennan, 1986; van de Plassche, 1986) of the deposits above and below the contact using the modern distribution of invertebrates as a guide (Fig. 4, Table 1).

In Carpinteria Marsh today, *C. californica* are found on the mudflats and high marsh surface (Bentz, 2016), which is consistent with previous studies that describe their elevation range as dominantly high intertidal (above mean sea level [MSL]) in the southwest Pacific coast (MacDonald, 1969a, 1969b; Sousa, 1983). Therefore, we estimate that the mud facies deposits below the contact formed between the paleoelevations of MLW and highest astronomical tide (HAT), a range which is slightly more conservative than that used for undifferentiated marsh deposits in other sea-level reconstructions from the Pacific coast of North America (Engelhart et al., 2015; Reynolds and Simms, 2015).

The bivalve species found above the contact within gray sand facies deposits occur at a wide range of elevations in estuaries and shallow coastal environments along the Pacific coast of North America (Fig. 4; Supplemental Material 4; see footnote 1), and their estuarine elevation ranges relative to tidal datums have not been systematically surveyed. However, the suite of species found in the gray sand facies are described as having “preferred” or “common” ranges in lower intertidal to subtidal environments (see Supplemental Material 4 and references therein);

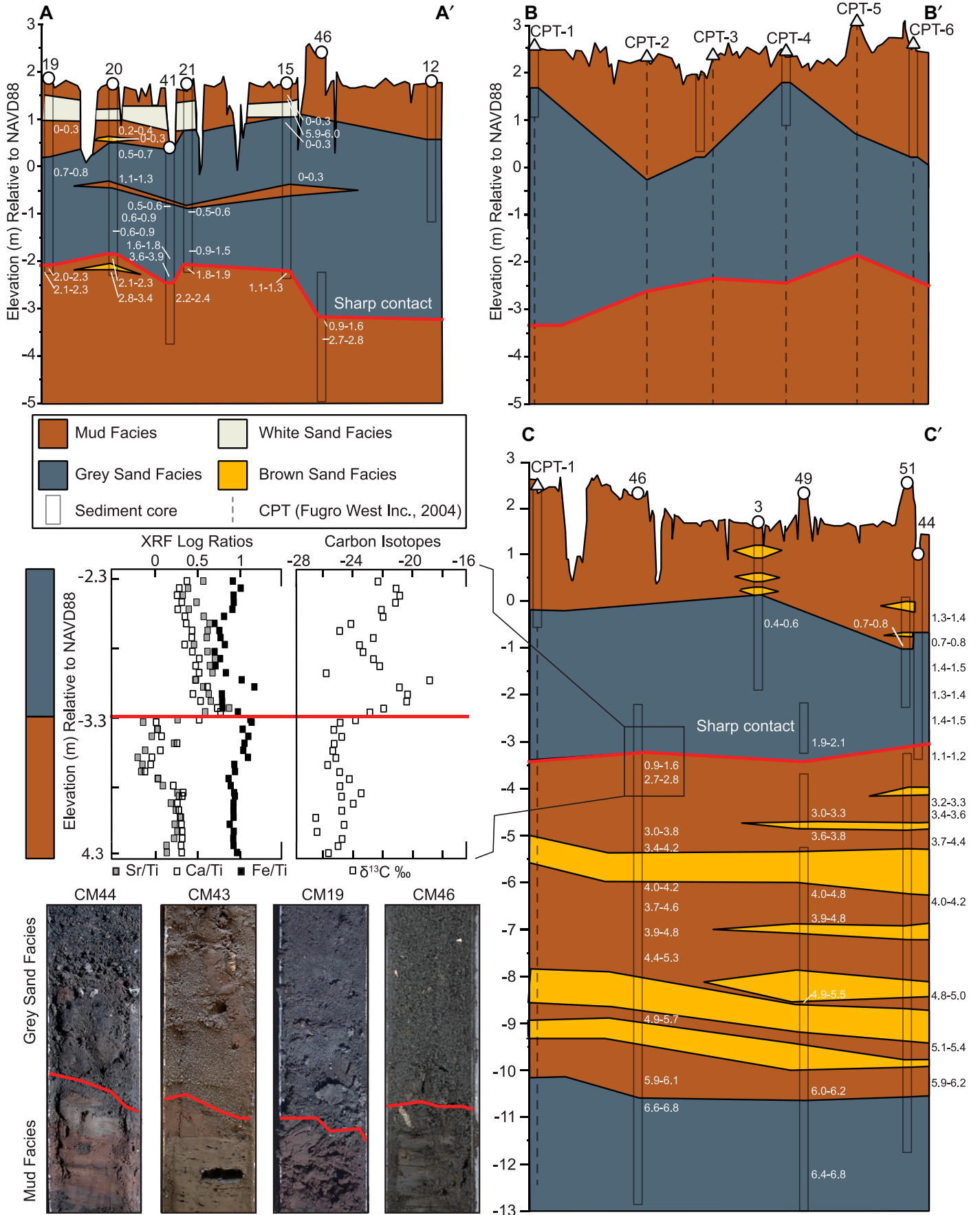


**Figure 3. Marsh stratigraphy and evidence for relative sea level change are shown. Shore-parallel core transect A, shore-parallel cone penetration test (CPT) transect B (redrawn based on Fugro West, 2004, Plate 4A), and shore-perpendicular core transect C. Grey boxes indicate the depth of material sampled in sediment cores; dotted lines indicate the depth of borehole CPT data (Fugro West, 2004). The stratigraphy based on data from the Fugro West (2004) report is interpreted here based on their interpretations of grain size; we assume that the deposits ~–3 to 1.5 m relative to NAVD88 described as dominantly sand in the Fugro West (2004) report are correlative with the bed we identify as gray sand facies, while those described as clay/silt/fine-grained are correlative with mud facies. Correlations of beds of brown sand facies are based on age and lithological data and are uncertain. Details of X-ray fluorescence and carbon isotopic data from Core 46 are shown below Transect A-A'. Radiocarbon ages are given in calibrated thousands of yr B.P., and the ranges shown have 2σ uncertainties. Several redundant radiocarbon ages from CM46 were removed for clarity; all ages are listed in Table S2 (see footnote 1).**



therefore, we estimate that the gray sand facies was deposited below MSL. Due to the wide depth range of the species present (Fitch, 1953), it is also not possible to determine a definitive lower bound for the gray sand facies. However, the species present in the gray sand facies have been historically common in estuaries and shallow intertidal environments in southern California (Crooks, 2001; Desmond et al., 2002; Novoa et al., 2016), and paleoecological studies suggest that intertidal salt and mud flats were more common prehistorically than open lagoon conditions in other estuaries in southern California (Beller et al., 2014); therefore, we estimate that the gray sand facies was deposited between the elevations of the lowest astronomical tide (LAT) and MSL, which is consistent with the indicative range used for undifferentiated lagoon/estuarine samples in the RSL reconstruction of Reynolds and Simms (2015). However, due to this uncertainty in elevation at which the gray sand facies was deposited, the calculated elevation change should be considered a minimum value.

The indicative ranges defined here are consistent with (1) other palaeoecological interpretations of the depth range of similar communities (i.e., Crooks, 2001); (2) indicative ranges defined in other Pacific coast sea-level studies (i.e., Engelhart et al., 2015); as well as (3) the

modern elevation distributions of these environments as surveyed in studies from other locations along the Pacific coast of North America (see Supplemental Material 4 and references therein). Marsh platforms in California marshes were found to dominantly occur at MHHW  $\pm$  0.5 m (the specific range depends on the tidal range of the individual marsh) (Thorne et al., 2018). In Carpinteria, the modern marsh platform (including Salicornia Marsh and mudflats) is found between MLW and MHHW. In Mugu Lagoon, just to the south of Carpinteria, the marsh platform ranges from MSL to  $>$  MHHW. Older literature also supports these interpretations. MacDonald (1969), who surveyed estuarine environments in California, found that marsh environments occurred between mean lower high water (MLHW) and extreme high water (EHW), which is approximately equivalent to mean high water (MHW) to highest astronomical tide (HAT).

Following other studies (Hawkes et al., 2010, 2011; Grand Pre et al., 2012; Woodroffe and Barlow, 2015), we use the modern elevations of relevant tidal datums (MLW and MSL from Carpinteria Marsh (Sadro et al., 2007); LAT and HAT from the Santa Barbara Station NOAA tide gauge (<https://tidesandcurrents.noaa.gov>; accessed September 2021, present tidal epoch data) to calculate the magnitude of RSL change at the contact as follows:

$$\text{RSL}\Delta = E_{\text{pre}} - E_{\text{post}} \quad (1)$$

where RSL $\Delta$  is magnitude of change in RSL,  $E_{\text{pre}}$  is the elevation, relative to MSL, of the below-contact marsh surface, and  $E_{\text{post}}$  is the elevation, relative to MSL, of the above-contact estuary surface.

The uncertainty in this calculation, RSL $\Delta_{\text{error}}$ , is determined as follows:

$$\text{RSL}\Delta_{\text{error}} = \text{sqrt}(E_{\text{pre,error}}^2 + E_{\text{post,error}}^2) \quad (2)$$

where  $E_{\text{pre,error}}$  is the indicative range of the mud facies deposits below the contact and  $E_{\text{post,error}}$  is the indicative range of the gray sand facies deposits above the contact. Following other studies (i.e., Hijma et al., 2015; Khan et al., 2019), this uncertainty is assumed to approximate a 2σ vertical error.

Using these calculations, the contact represents a 1.3  $\pm$  1.1 m rise in RSL; the characteristics described above suggest this rise in RSL caused a marsh/mudflat environment to transform to lower elevation intertidal sand flats. Because no abrupt rises in RSL have been inferred in late Holocene sea-level reconstructions for California (Reeder-Myers et al., 2015; Reynolds and Simms, 2015; Yousefi et al.,

2018), we interpret this rise in RSL to represent subsidence of the marsh surface. In addition, the irregular/sharp nature of the contact and presence of muddy rip up clasts in the gray sand facies deposits above the contact indicate that the contact-forming event was erosive, abrupt, and followed by high energy deposition.

### Chronology of the Contact

To place Carpinteria Marsh's sea level history in a regional context, we used each radiocarbon age from Carpinteria Marsh as a sea-level index point (Shennan, 1986; van de Plassche, 1986) with an indicative range indicated by the facies with which it is associated. We calculated the paleo RSL represented at each radiocarbon sample following the methods described in Reynolds and Simms (2015; Fig. 5). Unlike in Reynolds and Simms (2015), we did not apply a tectonic correction (to illustrate any tectonic effects on the marsh). Therefore, the vertical error includes uncertainty in the ground surface elevation and the indicative range; compaction was neglected. Radiocarbon ages show that sedimentation in Carpinteria Marsh was  $\sim$ 0.2 cm/yr from ca. 7–3 ka, which is consistent with regional rates of sea-level rise at that time (Yousefi et al., 2018), although all ages from mud facies deposits are at lower elevations than would be expected from the regional sea-level record (Fig. 5).

After ca. 3.0 ka, the sedimentary history among cores becomes more variable. Radiocarbon ages from samples in mud facies deposits just below the contact range from 1 ka to 3 ka over a limited vertical range (within 25 cm below the contact), which indicates erosion, non-deposition, or compaction of sediments from this time period. Ages from samples above the contact, from the gray sand facies deposits, are variable and often out of stratigraphic order within their core, which indicates reworking, or they have overlapping age ranges, which indicates rapid sedimentation. This variability in radiocarbon ages introduces significant uncertainty in the timing of development of the contact formation. Therefore, to test whether the contact formed synchronously and determine its age, we used two different methods, each of which has its own limitations and assumptions. Prior to running the age models, we removed seven ages that had two conditions indicative of reworking/contamination: (1) they were out of stratigraphic order within their core; and (2) the sample dated had other indications of reworking (small sample size, multiple fragments, evidence of bioturbation, etc.) or modern contamination (was described as a root) (Table S2).

First, we used the Bayesian age-depth model, Bacon (Blaauw and Christen, 2011), and

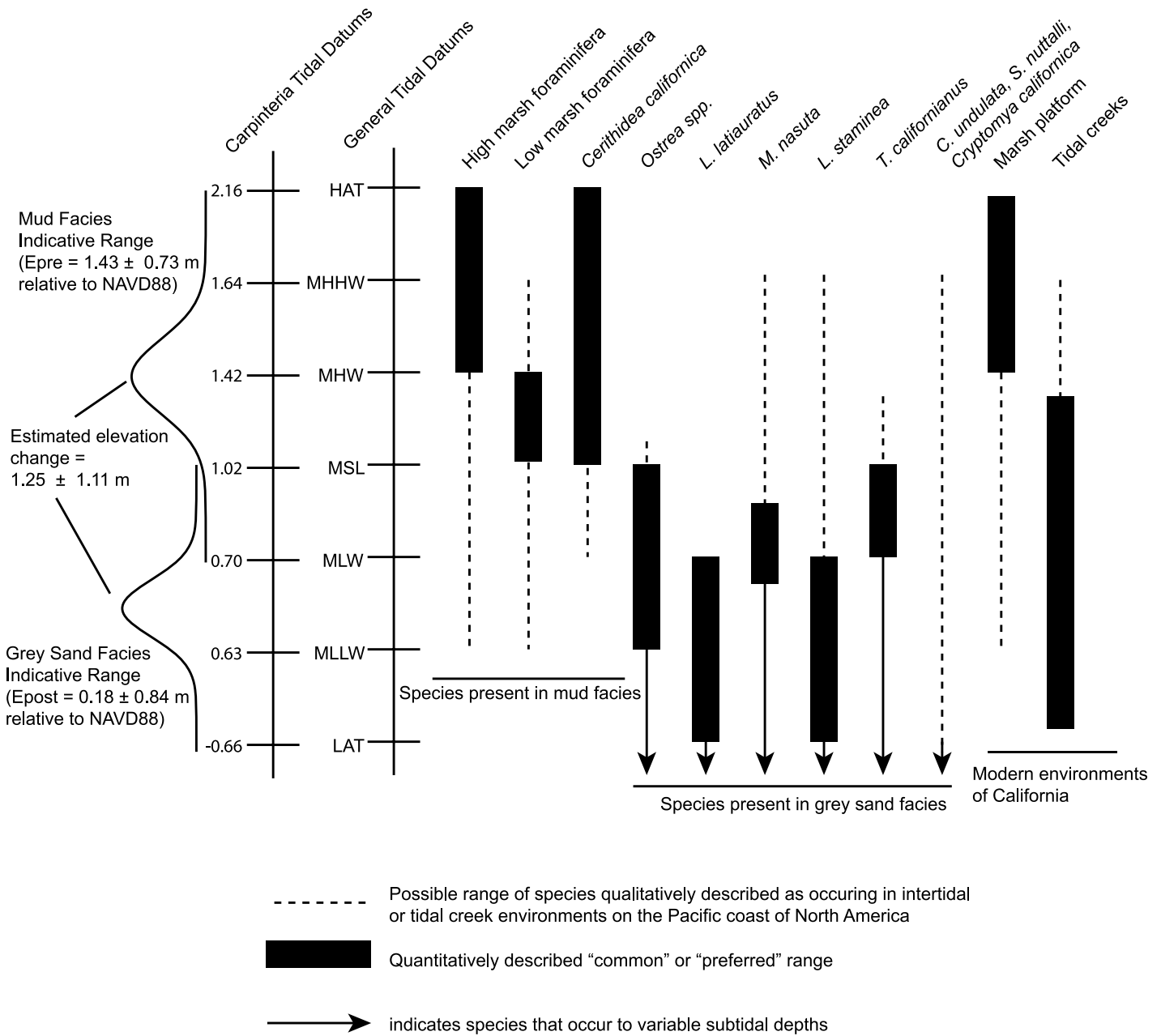


**Figure 4.** Species depth ranges were compiled from previously published reports from throughout the Pacific coast of North America (detailed in Supplemental Material 4; see footnote 1). Black boxes indicate ranges that are quantitatively indicated and described as “preferred,” “common,” or “high density.” Dashed lines indicate the possible range of the species, which is estimated from qualitative descriptions such as “intertidal” or “lower intertidal.” The local tidal datums relative to NAVD88 are shown on the left side of the figure; all of these measurements are from Sadro et al., 2007, except the two starred datums (LAT and HAT), for which Carpinteria-specific data was not available. LAT and HAT were taken from the National Oceanic and Atmospheric Administration Santa Barbara tide gauge (<https://tidesandcurrents.noaa.gov/datums.html?id=9411340>) datums from the present tidal epoch. The indicative ranges of mud facies and gray sand facies are equivalent to those in Equation 1. The terms Epre and Epost (estimated elevation prior to subsidence and estimated elevation post subsidence), respectively, are shown as estimated normal distributions with the 2σ range equivalent to the indicative range.

calculated the age of the contact separately in each of the six cores that continuously sampled across the contact and had ages both above and below it (Supplemental Material 3; see footnote 1). Because an erosional contact represents miss-

ing time, the age-depth model was set to assume a hiatus of unknown duration at the contact. Because of the lithological change at the contact, we assumed the sedimentation rates above and below the contact were independent. For all age-

depth models, a gamma distribution representing a mean accumulation rate of 0.4 cm/yr was used as the prior value for the sediments above the contact. This value is the average sedimentation rate previously calculated from Pb<sup>210</sup>, Cs<sup>137</sup>, and

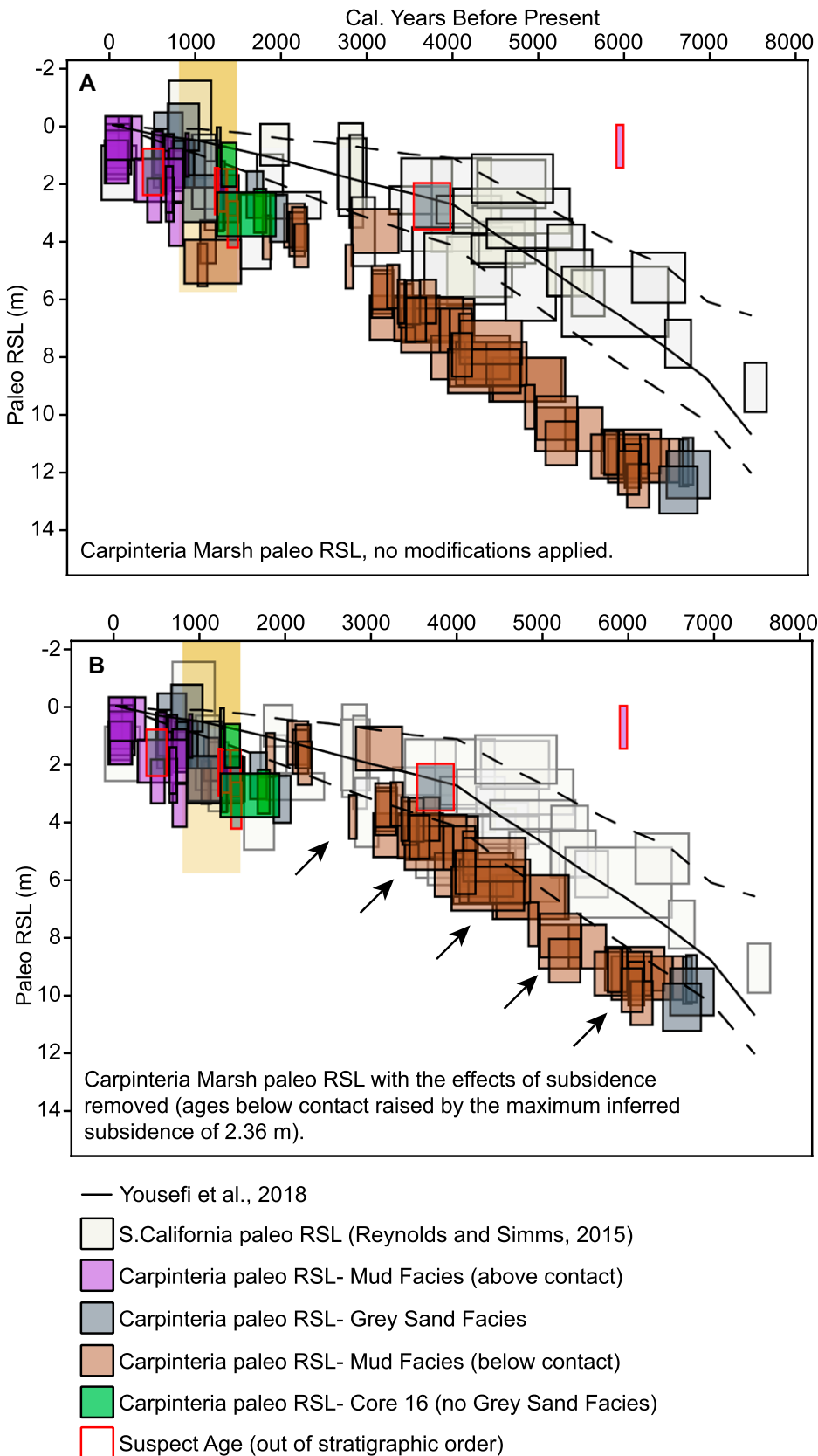


**Figure 5.** Paleo relative sea level from Carpinteria Marsh compared with paleo relative sea level data from southern California (Reynolds and Simms 2015) are shown. (A) The  $2\sigma$  calibrated radiocarbon ages vs. paleo relative sea level (RSL) (calculated following Reynolds and Simms, 2015) are shown relative to present mean sea level (MSL) in all cores. The vertical uncertainty is indicated by the height of the box and represents an  $\sim 2\sigma$  uncertainty, which includes the indicative range of the sample and the uncertainty in the ground surface elevation for each core, which was less than 0.15 m for all samples. The black lines show the bounds of a glacial isostatic adjustment (GIA) RSL model of southern California from Yousefi et al. (2019), which was fit to paleo RSL data for other sites in southern California from Reynolds and Simms (2015) (shown as gray boxes). (B) The same data are shown but with the Carpinteria ages beneath the contact raised by the maximum inferred subsidence of 2.36 m to test whether the removal of coseismic displacement places Carpinteria's paleo RSL within that calculated for southern California.

pollen/pollution horizons (Reynolds et al., 2018) for the upper 1–2 m of sediment in Carpinteria Marsh. The prior value used for the accumulation rate of sediments below the contact was 0.2 cm/yr, which is the sedimentation rate we calculated from a linear regression of all calibrated ages and depths below NAVD88 values below the contact ( $[\text{depth relative to NAVD88 (cm)}] = 0.2 \text{ cm/yr} * [\text{cal yr B.P.}] + 149 \text{ cm}$ ,  $R^2 = 0.93$ ). The stratigraphy above and below the contact (the presence of beds of brown sand facies and spatial variability in the thickness of the gray sand facies deposits) indicates that sedimentation is temporally variable; however, the average sedimentation rates used for the priors result in age-depth models that fit the observed ages reasonably well (see Supplemental Material 3).

Using separate chronologies for each core (no synchronicity is assumed between cores), the contact dates to (mean and  $2\sigma$  range, cal yr B.P.):  $0.9 \pm 0.2$  ka (CM15),  $1.2 \pm 0.2$  ka (CM20),  $1.2 \pm 0.2$  ka (CM19),  $0.9 \pm 0.2$  ka (CM21),  $1.1 \pm 0.1$  ka (CM41), and  $1.1 \pm 0.1$  ka (CM44). Each age-depth model relies on a very limited number of ages; therefore, the possible presence of inherited ages (not identified as such) or a greater degree of erosion in some cores may bias their age models towards

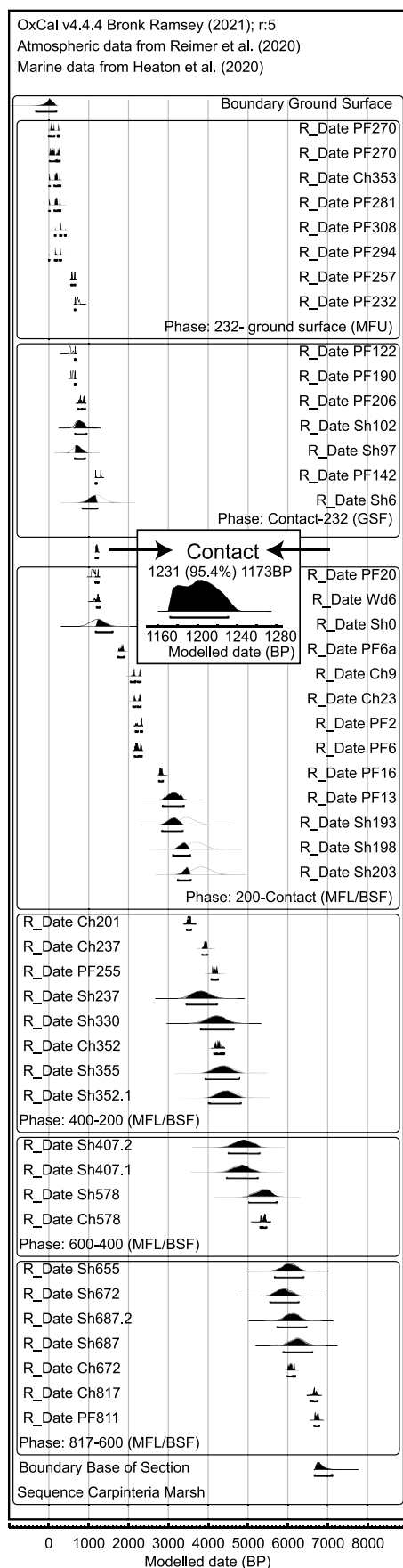


**Figure 6.** C. Bronk Ramsey, OxCal 4.4.4. Available from: <http://c14.arch.ox.ac.uk/oxcal> (2021) calibrated  $2\sigma$  ages are shown relative to the contact and the model of contact age. Black distributions are posterior (calibrated) probability density functions, and white outlines are likelihood distributions based on given radiocarbon ages (Bronk Ramsey, 2009). Ages from a similar stratigraphic position relative to the contact and within the same facies were grouped into phases as indicated by the black boxes Lienkaemper and Bronk Ramsey (2009). Terrestrial samples were calibrated in OxCal using IntCal20 (Reimer et al., 2020), and shell samples were calibrated in OxCal using Marine20 (Heaton et al., 2020) using estuarine marine reservoir values from Holmquist et al. (2015) updated with the Marine20 Reservoir Database (<http://calib.org/marine/>; accessed September 2021). See Table S2 (footnote 1) for radiocarbon sample details and reservoir values used for shell samples. The name of each R\_Date indicates the type of material and its depth relative to the contact, i.e., PF811 = plant fragment from 811 cm below the contact. For ages below the contact (listed first in the script), the depth should be read as “centimeters below the contact,” while for ages above the contact (listed further down in the script), the depth given should be read as “centimeters above the contact.” PF—plant fragment; Sh—shell; Ch—charcoal; Wd—wood. Additional details about the radiocarbon ages and reservoir values are provided in Table S2 and in the text. MFU—mud facies, upper (above contact); GSF—gray sand facies; MFL/BSF—mud facies, lower/brown sand facies (below contact).

older ages, contributing to variability in the age models among cores. Regardless, the ranges of the modeled ages of the contact overlap, which suggests that the contact formed synchronously across the marsh between 0.7 ka and 1.4 ka.

Because the Bacon age-depth models use assumptions about sedimentation rates and require us to identify the contact as a hiatus for the model to recognize it as such, we also calculated the age of the contact using the Bayesian age-depth model OxCal v4.4.4 (Lienkaemper and Bronk Ramsey, 2009; Bronk Ramsey, 2009), which (when using the Sequence and Phase functions) requires assumptions about stratigraphic order but not sedimentation rates. In this model, we used 47 radiocarbon ages from seven cores that continuously sampled across the contact, because their vertical distance from the contact could be established. Following Lienkaemper and Bronk Ramsey (2009), we grouped data from multiple cores into a single stratigraphic package (same facies and similar depth relative to contact) termed a “Phase” in the program. The ages within each phase were not constrained to a particular order in the model (although they are shown in chronological order for clarity in Fig. 6), but the phases themselves are constrained to be sequential—i.e., the stratigraphically lower phases are assumed to have occurred before those stratigraphically above them. Based on this model, the contact formed at 1173–1231 cal yr B.P. ( $2\sigma$  age range), which overlaps the contact age modeled using Bacon. However, any inherited ages that may remain in the gray sand facies phase above the contact could bias this model toward older ages. Therefore, we consider this modeled age to be a maximum. Taken together, the Bacon and OxCal models give overlapping age estimates

for the submergence event and suggest the contact formed between 0.7 ka and 1.3 ka, which is hereafter given as  $1.0 \pm 0.3$  ka (representing the midpoint and range of possible ages). The plethora of ages above the contact between 0.5 ka and 1 ka qualitatively supports this interpretation and suggests that sediment started rapidly accumulating sometime after 1 ka.

The landward limit of deposition of gray sand facies (and therefore long-lasting, post-seismic flooding) is indicated by the lack of gray sand facies deposits in several cores around the landward margins of the marsh (Fig. 2). The deepest of these cores, CM16, extends to 4 m depth below ground surface (1.6 m relative to NAVD88). This core contains a bed of brown sand facies with convolute bedding (Supplemental Material 1, Fig. S3) that was possibly produced by earthquake-induced liquefaction, which dates to  $0.9 \pm 0.1$  ka ( $2\sigma$  uncertainty, based on a separate Bacon age-depth model) and overlaps the time of formation of the contact. The lack of marine-influenced sand above this layer suggests that CM16 subsided from a higher pre-subsidence elevation and remained above MSL after subsidence or was subjected to less erosion and compaction than sediments from more seaward parts of the marsh.

## DISCUSSION

### Interpretation of the Contact

The evidence presented above suggests that the contact formed synchronously across the marsh at ca.  $1.0 \pm 0.3$  ka due to an abrupt deepening of a marsh/mudflat environment that initiated rapid and high-energy deposition of gray sand facies deposits in an intertidal to subtidal

setting. The data presented are consistent with many of the criteria described elsewhere (Nelson et al., 1996, 1998; Shennan et al., 2016) as indicative of coseismic subsidence: a laterally extensive and sharp contact, evidence of an RSL rise, and evidence of synchronicity of change that is replicated in multiple cores. In addition, the paleo RSL values calculated for Carpinteria Marsh consistently fall below what would be expected based on the paleo RSL calculated for other sites in southern California from 3 ka to 7 ka. If we raise the sea-level index points below the contact by the maximum inferred subsidence amount (Fig. 5B), the modified paleo RSL ranges (while highly uncertain) overlap the lower part of the range in RSL values inferred for southern California (Reynolds and Simms, 2015; Yousefi et al., 2018). However, the Carpinteria values are still generally lower than those from other estuaries in southern California, which perhaps indicates additional subsidence from compaction.

Carpinteria Marsh is located on the downthrown side of the Rincon Creek Fault (Jackson and Yeats, 1982), which offsets Quaternary gravels on shore (Dibblee, 1994; Fredrickson, 2016; Jackson and Yeats, 1982). Therefore, movement on this fault is likely the source of the subsidence observed, and we argue that, while not a unique solution, coseismic subsidence is the most consistent explanation for the available data. However, nonseismic processes, such as floods, mouth or tidal channel migration, climate change-related sedimentation changes, or barrier breaching events can cause stratigraphic changes similar to those created by coseismic subsidence (Nelson et al., 1998, 1996). In the section below, we argue that the evidence is inconsistent with these alternative scenarios.

The ages of several large flood events recorded in the Santa Barbara Channel sedimentary record (Hendy et al., 2013) overlap the age of deposition of the upper bed of gray sand facies in Carpinteria Marsh. However, the gray sand facies deposits above the contact are bioturbated and contain radiocarbon dates that span 500 years of deposition, which indicates that this deposit represents a period of long-lasting environmental change and not a single event. Additionally, if the deposits of gray sand facies represented storm driven deposition, the repetition of flood layers in the Santa Barbara Basin (Du et al., 2018) would suggest that multiple beds of gray sand facies should be present in the deeper cores, which we do not observe.

Tidal channel, mouth migration, or a transgressing shoreline could form a contact similar to that described here; however, these processes would be expected to cause progressive erosion throughout the marsh. For example, a transgressing shoreline would be expected to be more ero-

sive oceanward and less erosive landward and therefore would be underlain by ages that young landward. In Carpinteria Marsh, the variable ages that underlie the contact exhibit no clear pattern relative to geography. The depth of the contact varies spatially (from  $-1.9$  to  $-3.3$  m relative to present MSL) and deepens in the direction of the area of greatest offset on the Rincon Creek Fault (Jackson and Yeats, 1982), which may reflect a combination of differential subsidence, irregularity of the original marsh surface, and spatial variability in erosion and/or compaction related to the subsidence event.

One possible explanation for the observed lack of radiocarbon ages between 1 ka and 3 ka would be a decrease in sedimentation during this time due to climatic changes that resulted in non-accumulation and/or erosion of the marsh for ca. 2000 years before abruptly resuming sedimentation at 1.0 ka. However, at least four small streams prehistorically drained into Carpinteria Marsh; therefore, a hiatus in sediment deposition by these streams would require all entering streams to avulse away from the marsh at once, which would be unlikely. If a large-scale shift in climate were responsible, we would expect to see similar, contemporaneous responses from other estuaries in southern California—which does not appear to be the case from existing paleoecological records (Cole and Wahl, 2000; Ejarque et al., 2015; Lohmar et al., 1980). Instead, the erosion/nondeposition indicated from 1 ka to 3 ka likely reflects a combination of decreased sediment accumulation due to sea-level deceleration (Reynolds and Simms, 2015; Yousefi et al., 2018) as well as erosion and compaction induced by the subsidence event itself. Compaction/consolidation of surficial sediments has been documented in historical subsidence events (Plafker, 1969; Weischet, 1963).

Finally, the contact could be attributed to abrupt breaching of a sandy barrier that previously sheltered the estuary from marine influence (Nelson, 1992). Any scenario that does not call on tectonic subsidence, such as barrier breaching and all other alternatives mentioned previously, would require that the mud facies deposits below the contact were deposited  $\sim 1$ – $3$  m below MSL from 7 ka to 3 ka (see discrepancy between ages from Carpinteria Marsh sediment and the regional RSL curve in Fig. 5). However, the geochemical characteristics of the mud facies deposits and the presence of *C. californica* suggest that the mud facies sediments were deposited in an intertidal environment above MLW. Additionally, the environmental change represented by the contact appears to be laterally continuous and synchronous across much of the modern marsh and possibly beyond its present boundaries, which would be difficult to accomplish

in a single barrier breach. Therefore, we argue that coseismic subsidence is the most consistent explanation for the available data.

### Hazard Implications

If a subsidence event were to recur today along the highly populated Santa Barbara coast, effects would include coastal flooding, ecological community shifts, damage to infrastructure due to liquefaction, and increased susceptibility of low-lying coastal areas to storms and sea-level rise (Hughes et al., 2015; Imakiire and Koarai, 2012; Jaramillo et al., 2017). However, the linear sedimentation rate from 3 ka to 7 ka and the absence of stratigraphic evidence for older subsidence events suggests that the recurrence interval for large, coseismic subsidence in Carpinteria may be greater than 6 k.y. or that previous coseismic events did not result in an environmental change large enough to be identified in the stratigraphy.

The most likely source of subsidence within Carpinteria Marsh is movement along the Rincon Creek Fault as a backthrust event off a larger fault in the region (Levy et al., 2019). The age range for the Carpinteria subsidence event overlaps that of the most recent large earthquake at Pitas Point near Ventura, which is dated to ca.  $0.95^{+0.14/-0.11}$  ka (Rockwell et al., 2016). Assuming these two events are correlated would support the potential for large-scale ruptures within the Ventura/Santa Barbara regions. However, no other stratigraphic changes clearly indicative of uplift or subsidence are present in the Carpinteria record, while three other uplift events that occurred during the past 7000 years have been documented at Pitas Point. This discrepancy may suggest that movement along the larger thrust faults in the region only occasionally activates the Rincon Creek Fault or that previous subsidence events were too small to be recognized in the stratigraphy.

### Sedimentary Response of Structural Estuaries to Subsidence

The Carpinteria estuary responded to the coseismic increase in accommodation with a rapid accumulation of intertidal sediments (gray sand facies), which is similar to the responses of estuaries observed after historical coseismic events (Atwater et al., 2001; Ovenshine et al., 1976; Weischet, 1963) and well-dated prehistorical events in the stratigraphic record (Atwater and Hemphill-Haley, 1997; Benson et al., 2001). The characteristics of the gray sand facies sediments suggest they were deposited in a high-energy tidal sand flat environment formed over the prior marsh and mudflat deposits (mud facies). The presence of marine species

and silt-sand couplets in the gray sand facies deposits reflects an increased tidal influence after subsidence that perhaps represents a temporary increase in the tidal range as the estuary deepened and became more open to the ocean. However, as indicated by the lack of gray sand facies deposits in CM16 and the variability in the depth of the contact, the effects of coseismic subsidence varied throughout the marsh perhaps due to variations in the pre-subsidence elevation as well as post-subsidence erosion and compaction.

Although the radiocarbon data suggest a rapid accumulation of intertidal sediments immediately following the subsidence event, the gradual shoaling of the estuary to its pre-subsidence elevation ultimately lasted 500–900 years, which is consistent with observations (Atwater et al., 2001; Benson et al., 2001; Reinhardt et al., 2010) that estuaries with smaller tidal ranges take longer to recover (in terms of their elevations) from coseismic subsidence than those with larger tidal ranges and therefore would not as readily preserve evidence of temporally close events. This lag was likely exacerbated in Carpinteria by the Mediterranean climate and lack of large river influences, which limited the input of fluvial sediments, in contrast to the rapid accumulation of deltaic and fluvial deposits observed following subsidence events in estuaries and wetlands fed by permanent streams (Clark et al., 2013; Cochran et al., 2017; Knudsen et al., 2002; Reinhardt et al., 2010).

The displacement of the paleomorph surface deposits relative to their expected elevations based on regional RSL (Reynolds and Simms, 2015; Fig. 5) is consistent with the results of other studies (Castro et al., 2010; Chelli et al., 2017; Clement and Fuller, 2018; Hayward et al., 2010; Rodriguez-Ramírez et al., 2014; Simms et al., 2016; Tanabe et al., 2013) that indicate that structural estuaries contain thicker deposits of intertidal and alluvial sediments than would be expected from non-tectonic increases in accommodation alone. Coseismic subsidence also displaces older deposits downward, which increases their preservation potential. Previous research on the deep structure of the Carpinteria basin (Jackson and Yeats, 1982) suggests that it has been subsiding since the middle Quaternary. To accommodate the structure and depth of the basin, it is likely that the estuary has experienced many other coseismic events over its lifetime and preserves sediments from previous transgressions and highstands as observed in other structural estuaries (Atwater et al., 1977).

## CONCLUSIONS

Previous studies have argued that accommodation created by RSL rise is a prerequisite for

stratigraphic preservation of coseismic events and that evidence of coseismic subsidence is not as well-preserved during times of RSL stagnation or fall (Dura et al., 2016; Kelsey et al., 2015). However, many of these studies focus on estuaries in subducting regions where elastic deformation and/or interseismic uplift can decrease the permanent vertical change generated by subsidence. In contrast, deformation in Carpinteria, and in other structurally bound estuaries (Atwater et al., 1977; Simms et al., 2016), may result in non-elastic, permanent deformation. In Carpinteria, coseismic subsidence may have temporarily interrupted the typical maturation process described in classic estuarine facies models (Boyd, 2006; Dalrymple et al., 1992); it is possible that without late Holocene subsidence, Carpinteria Marsh may have transitioned from an estuary to a delta as RSL rise decelerated in the late Holocene. Future studies could test whether these implications are broadly applicable to other structurally controlled estuaries and whether structural estuaries contain stratigraphic evidence of environmental changes and deformation events independent of the trajectory of the concurrent non-tectonic components of RSL.

This research indicates that abrupt, coseismic subsidence in fault-bounded estuaries in regions such as the Californian, Mediterranean, and other active coastlines, can be identified and quantified in the stratigraphic record using the same, well-established criteria as those used to differentiate subsidence from other estuarine processes along subduction and strike-slip margins. This study follows a long line of previous studies from active margins around the world that have demonstrated that accommodation created by tectonic subsidence, in addition to non-tectonic RSL rise, results in distinctive sedimentary and stratigraphic characteristics of active margin estuaries, such as high long-term rates of sedimentation, evidence for abrupt rises in RSL, and a recovery response that is dependent on sediment influx and tidal range. The identification of localized subsidence events in structural estuaries can help elucidate seismic hazards and may provide additional insights into subsurface relationships in complicated tectonic regions.

## ACKNOWLEDGMENTS

This research was supported by the Southern California Earthquake Center, USA, (Contribution No. 7942; Grants No. 14008 and 15156), the Santa Barbara Coastal Long Term Ecological Research (LTER) project (California, USA), and the Japan Society for the Promotion of Science (JSPS KAKENHI, JP15KK0151 and JP17H01168). SCEC is funded by U.S. National Science Foundation Cooperative Agreement EAR-1033462 and U.S. Geological Survey Cooperative Agreement G12AC20038. This material is based upon work supported by the National Science

Foundation Graduate Research Fellowship under Grant No. DGE-1144085. We thank our field and lab assistants, as well as Andrew Brooks, Chanda Bertrand, John Southon, David Griggs, Craig Nicholson, and Paul-Valentich Scott. We also thank the several anonymous reviewers whose thoughtful and constructive comments have vastly improved this manuscript.

## REFERENCES CITED

- Addison, J.A., Finney, B.P., Jaeger, J.M., Stoner, J.S., Norris, R.D., and Hangsterfer, A., 2013, Integrating satellite observations and modern climate measurements with the recent sedimentary record: An example from Southeast Alaska: *Journal of Geophysical Research: Oceans*, v. 118, no. 7, p. 3444–3461, <https://doi.org/10.1002/jgrc.20243>.
- Atwater, B.F., 1987, Evidence for great Holocene earthquakes along the outer coast of Washington State: *Science*, v. 236, no. 4804, p. 942–944, <https://doi.org/10.1126/science.236.4804.942>.
- Atwater, B.F., and Hemphill-Haley, E., 1997, Recurrence intervals for great earthquakes of the past 3,500 years at northeastern Willapa Bay, Washington: U.S. Geological Survey Professional Paper 1576, 108 p.
- Atwater, B.F., Hedel, C.W., and Helley, E.J., 1977, Late Quaternary Depositional History, Holocene Sea-Level Changes, and Vertical Crust Movement, Southern San Francisco Bay, California: U.S. Geological Survey Professional Paper 1014, 15 p., 1 plate.
- Atwater, B.F., Yamaguchi, D.K., Bondevik, S., Barnhardt, W.A., Amidon, L.J., Benson, B.E., Skjerdal, G., Shulene, J.A., and Nanayama, F., 2001, Rapid resetting of an estuarine recorder of the 1964 Alaska earthquake: *Geological Society of America Bulletin*, v. 113, no. 9, p. 1193–1204, [https://doi.org/10.1130/0016-7606\(2001\)113<1193:RROAER>2.0.CO;2](https://doi.org/10.1130/0016-7606(2001)113<1193:RROAER>2.0.CO;2).
- Avnaim-Katav, S., Gehrels, W.R., Brown, L.N., Fard, E., and MacDonald, G.M., 2017, Distributions of salt-marsh foraminifera along the coast of SW California, USA: Implications for sea-level reconstructions: *Marine Micropaleontology*, v. 131, p. 25–43, <https://doi.org/10.1016/j.marmicro.2017.02.001>.
- Bakker, E., and Slack, G., 1984, *An Island Called California: An Ecological Introduction to its Natural Communities*: Oakland, California, USA, University of California Press, 512 p.
- Beller, E.B.S., Grossinger, R.M., Longcore, T., Stein, E.D., Dark, S., and Dusterhoff, S.D., 2014, Northern San Diego County Lagoons Historical Ecology Investigation: Regional Patterns, Local Diversity, and Landscape Trajectories (Prepared for the State Coastal Conservancy): Richmond, California, USA, SFEI Publication 722, San Francisco Estuary Institute, 119 p.
- Benson, B.E., Atwater, B.F., Yamaguchi, D.K., Amidon, L.J., Brown, S.L., and Lewis, R.C., 2001, Renewal of tidal forests in Washington State after a subduction earthquake in AD 1700: *Quaternary Research*, v. 56, no. 2, p. 139–147, <https://doi.org/10.1006/qres.2001.2251>.
- Bentz, M., 2016, Establishing foraminifera-based biofacies within shallow marine deposits, Carpinteria Slough, CA. Implications for southern California sea-level studies [M.S. thesis]: Santa Barbara, California, USA, University of California Santa Barbara.
- Blaauw, M., and Christen, J.A., 2011, Flexible paleoclimate age-depth models using an autoregressive gamma process: *Bayesian Analysis*, v. 6, no. 3, p. 457–474, <https://doi.org/10.1214/ba/1339616472>.
- Bourgeois, J., and Johnson, S.Y., 2001, Geologic evidence of earthquakes at the Snohomish delta, Washington, in the past 1200 yr: *Geological Society of America Bulletin*, v. 113, no. 4, p. 482–494, [https://doi.org/10.1130/0016-7606\(2001\)113<0482:GEOEAT>2.0.CO;2](https://doi.org/10.1130/0016-7606(2001)113<0482:GEOEAT>2.0.CO;2).
- Boyd, R., 2006, Estuarine and incised-valley facies models: Facies Models Revisited, v. 84, p. 171–235.
- Bronk-Ramsey, C., 2009, Bayesian analysis of radiocarbon dates: *Radiocarbon*, v. 51, no. 1, p. 337–360, <https://doi.org/10.1017/S0033822200033865>.
- Castro, D.F., de Fátima Rossetti, D., and Pessenda, L.C.R., 2010, Facies,  $\delta^{13}\text{C}$ ,  $\delta^{15}\text{N}$  and C/N analyses in a late

- Quaternary compound estuarine fill, northern Brazil and relation to sea level: *Marine Geology*, v. 274, no. 1–4, p. 135–150, <https://doi.org/10.1016/j.margeo.2010.03.011>.
- Chagué-Goff, C., Szczuciński, W., and Shinozaki, T., 2017, Applications of geochemistry in tsunami research: A review: *Earth-Science Reviews*, v. 165, p. 203–244, <https://doi.org/10.1016/j.earscirev.2016.12.003>.
- Chelli, A., Pappalardo, M., Bini, M., Bruckner, H., Neri, G., Neri, M., and Spada, G., 2017, Assessing tectonic subsidence from estimates of Holocene relative sea-level change: An example from the NW Mediterranean (Magra Plain, Italy): *The Holocene*, v. 27, no. 12, p. 1988–1999, <https://doi.org/10.1177/0959683617715688>.
- Clark, K., Cochran, U., Berryman, K., Biasi, G., Langridge, R., Villamor, P., Bartholomew, T., Litchfield, N., Pantostis, D., and Marco, S., 2013, Deriving a long paleoseismic record from a shallow-water Holocene basin next to the Alpine fault, New Zealand: *Geological Society of America Bulletin*, v. 125, no. 5–6, p. 811–832, <https://doi.org/10.1130/B30693.1>.
- Clement, A.J.H., and Fuller, I.C., 2018, Influence of system controls on the Late Quaternary geomorphic evolution of a rapidly-infilled incised-valley system: The lower Manawatu valley, North Island New Zealand: *Geomorphology*, v. 303, p. 13–29, <https://doi.org/10.1016/j.geomorph.2017.11.016>.
- Cochran, U., Clark, K., Howarth, J., Biasi, G., Langridge, R., Villamor, P., Berryman, K., and Vandergoes, M., 2017, A plate boundary earthquake record from a wetland adjacent to the Alpine fault in New Zealand refines hazard estimates: *Earth and Planetary Science Letters*, v. 464, p. 175–188, <https://doi.org/10.1016/j.epsl.2017.02.026>.
- Cole, K.L., and Wahl, E., 2000, A Late Holocene Paleocological Record from Torrey Pines State Reserve, California: *Quaternary Research*, v. 53, no. 3, p. 341–351, <https://doi.org/10.1006/qres.1999.2121>.
- Crooks, J.A., 2001, Assessing invader roles within changing ecosystems: Historical and experimental perspectives on an exotic mussel in an urbanized lagoon: *Biological Invasions*, v. 3, no. 1, p. 23–36, <https://doi.org/10.1023/A:1011404914338>.
- Cundy, A., Kortekaas, S., Dewez, T., Stewart, I., Collins, P., Croudace, I., Maroukian, H., Papanastassiou, D., Gaki-Papanastassiou, P., and Pavlopoulos, K., 2000, Coastal wetlands as recorders of earthquake subsidence in the Aegean: A case study of the 1894 Gulf of Atalanti earthquakes, central Greece: *Marine Geology*, v. 170, no. 1, p. 3–26, [https://doi.org/10.1016/S0025-3227\(00\)00062-1](https://doi.org/10.1016/S0025-3227(00)00062-1).
- Dalrymple, R.W., Zaitlin, B.A., and Boyd, R., 1992, Estuarine facies models: Conceptual basis and stratigraphic implications: *Perspective: Journal of Sedimentary Research*, v. 62, no. 6, p. 1130, <https://doi.org/10.1306/D4267A69-2B26-11D7-8648000102C1865D>.
- Darizenzo, M.E., and Peterson, C.D., 1990, Episodic tectonic subsidence of late Holocene salt marshes, northern Oregon central Cascadia margin: *Tectonics*, v. 9, no. 1, p. 1–22, <https://doi.org/10.1029/TC009i001p00001>.
- Desmond, J., Deuschman, D., and Zedler, J., 2002, Spatial and temporal variation in estuarine fish and invertebrate assemblages: Analysis of an 11-year data set: *Estuaries*, v. 25, no. 4, p. 552–569, <https://doi.org/10.1007/BF02804890>.
- Dibblee, T.W., Jr., 1994, *Geology of the Carpinteria-Rincon Creek Area Santa Barbara and Ventura Counties, California*: Abstract presented at American Association of Petroleum Geologists Pacific Section Groundwater Geology of the Wine Country, Carpinteria and Santa Ynez Valley Region, Santa Barbara County, California, p. 23–27.
- Du, X., Hendy, I., and Schimmelmann, A., 2018, A 9000-year flood history for Southern California: A revised stratigraphy of varved sediments in Santa Barbara Basin: *Marine Geology*, v. 397, p. 29–42, <https://doi.org/10.1016/j.margeo.2017.11.014>.
- Dura, T., Engelhart, S.E., Vacchi, M., Horton, B.P., Kopp, R.E., Peltier, W.R., and Bradley, S., 2016, The role of Holocene relative sea-level change in preserving records of subduction zone earthquakes: *Current Climate Change Reports*, v. 2, no. 3, p. 86–100, <https://doi.org/10.1007/s40641-016-0041-y>.
- Ejarque, A., Anderson, R.S., Simms, A.R., and Gentry, B.J., 2015, Prehistoric fires and the shaping of colonial transported landscapes in southern California: A paleoenvironmental study at Dune Pond, Santa Barbara County: *Quaternary Science Reviews*, v. 112, p. 181–196, <https://doi.org/10.1016/j.quascirev.2015.01.017>.
- Engelhart, S.E., Vacchi, M., Horton, B.P., Nelson, A.R., and Kopp, R.E., 2015, A sea-level database for the Pacific coast of central North America: *Quaternary Science Reviews*, v. 113, p. 78–92, <https://doi.org/10.1016/j.quascirev.2014.12.001>.
- Ferren, W.R., 1985, *Carpinteria Salt Marsh: Environment, history, and botanical resources of a southern California estuary*: Santa Barbara, California, USA, Department of Biological Sciences, University of California, Santa Barbara, Publication 4, 293 p., <https://doi.org/10.5962/bhl.title.63944>.
- Fitch, J.E., 1953, *Common Marine Bivalves of California*: State of California Department of Fish and Game Marine Fisheries Branch, Fish Bulletin 90, 102 p. (available at <https://escholarship.org/uc/item/1k431755>).
- Fredrickson, S., 2016, *The Geomorphic Transition between the Santa Barbara and Ventura Fold Belts near Rincon Point, California* [M.S. thesis]: Santa Barbara, California, USA, University of California, Santa Barbara, 114 p.
- Fugro West, L., 2004, *Geotechnical report Carpinteria Salt Marsh enhancement confluence of Franklin and Santa Monica Creeks Carpinteria California*, in District, S. B. C. F. C., ed.: Santa Maria, California, Fugro West Inc. for the Santa Barbara County Flood Control District, p. 1–27.
- Grand Pre, C.A., Horton, B.P., Kelsey, H.M., Rubin, C.M., Hawkes, A.D., Daryono, M.R., Rosenberg, G., and Culver, S.J., 2012, Stratigraphic evidence for an early Holocene earthquake in Aceh, Indonesia: *Quaternary Science Reviews*, v. 54, p. 142–151, <https://doi.org/10.1016/j.quascirev.2012.03.011>.
- Hawkes, A.D., Horton, B.P., Nelson, A.R., and Hill, D.F., 2010, The application of intertidal foraminifera to reconstruct coastal subsidence during the giant Cascadia earthquake of AD 1700 in Oregon, USA: *Quaternary International*, v. 221, no. 1–2, p. 116–140, <https://doi.org/10.1016/j.quaint.2009.09.019>.
- Hawkes, A.D., Horton, B., Nelson, A., Vane, C., and Sawai, Y., 2011, Coastal subsidence in Oregon, USA, during the giant Cascadia earthquake of AD 1700: *Quaternary Science Reviews*, v. 30, no. 3–4, p. 364–376, <https://doi.org/10.1016/j.quascirev.2010.11.017>.
- Hayward, B.W., Wilson, K., Morley, M.S., Cochran, U., Grenfell, H.R., Sabaa, A.T., and Daymond-King, R., 2010, Microfossil record of the Holocene evolution of coastal wetlands in a tectonically active region of New Zealand: *The Holocene*, v. 20, no. 3, p. 405–421, <https://doi.org/10.1177/0959683609353431>.
- Heaton, T.J., Köhler, P., Butzin, M., Bard, E., Reimer, R.W., Austin, W.E., Ramsey, C.B., Grootes, P.M., Hughen, K.A., and Kromer, B., 2020, Marine20—the marine radiocarbon age calibration curve (0–55,000 cal BP): *Radiocarbon*, v. 62, no. 4, p. 779–820, <https://doi.org/10.1017/RDC.2020.68>.
- Hendy, I.L., Dunn, L., Schimmelmann, A., and Pak, D.K., 2013, Resolving varve and radiocarbon chronology differences during the last 2000 years in the Santa Barbara Basin sedimentary record, California: *Quaternary International*, v. 310, p. 155–168, <https://doi.org/10.1016/j.quaint.2012.09.006>.
- Hijma, M.P., Engelhart, S.E., Törnqvist, T.E., Horton, B.P., Hu, P., and Hill, D.F., 2015, A protocol for a geological sea-level database, in Shennan, I., Long, A.J., and Horton, B.P., eds., *Handbook of Sea-Level Research*: Hoboken, New Jersey, USA, Wiley Blackwell, p. 536–553, <https://doi.org/10.1002/9781118452547.ch34>.
- Holmquist, J.R., Reynolds, L., Brown, L.N., Southon, J.R., Simms, A.R., and MacDonald, G.M., 2015, Marine radiocarbon reservoir values in southern California estuaries: Interspecies, latitudinal, and interannual variability: *Radiocarbon*, v. 57, no. 3, p. 449–458, [https://doi.org/10.2458/azu\\_rc.57.18389](https://doi.org/10.2458/azu_rc.57.18389).
- Hubbard, D.M., 1996, Tidal cycle distortion in Carpinteria salt marsh, California: *Bulletin of the Southern California Academy of Sciences*, v. 95, no. 2, p. 88–98.
- Hubbard, J., Shaw, J.H., Dolan, J., Pratt, T.L., McAuliffe, L., and Rockwell, T.K., 2014, Structure and seismic hazard of the Ventura Avenue anticline and Ventura fault, California: Prospect for large, multisegment ruptures in the western Transverse Ranges: *Bulletin of the Seismological Society of America*, v. 104, p. 1070, <https://doi.org/10.1785/0120130125>.
- Hughes, M.W., Quigley, M.C., van Ballegooy, S., Deam, B.L., Bradley, B.A., and Hart, D.E., 2015, The sinking city: Earthquakes increase flood hazard in Christchurch, New Zealand: *GSA Today*, v. 25, no. 3, p. 4–10, <https://doi.org/10.1130/GSATG221A.1>.
- Imakiire, T., and Koaari, M., 2012, Wide-area land subsidence caused by “the 2011 off the Pacific Coast of Tohoku Earthquake”: *Soil and Foundation*, v. 52, no. 5, p. 842–855, <https://doi.org/10.1016/j.sandf.2012.11.007>.
- Jackson, P.A., and Yeats, R.S., 1982, Structural evolution of Carpinteria basin, Western Transverse Ranges, California: *American Association of Petroleum Geologists Bulletin*, v. 66, no. 7, p. 805–829.
- Jaramillo, E., Melnick, D., Baez, J.C., Montecino, H., Lagos, N.A., Acuña, E., Manzano, M., and Camus, P.A., 2017, Calibrating coseismic coastal land-level changes during the 2014 Iquique ( $M_w = 8.2$ ) earthquake (northern Chile) with leveling, GPS and intertidal biota: *PLoS One*, v. 12, no. 3, p. e0174348, <https://doi.org/10.1371/journal.pone.0174348>.
- Johnson, S.Y., Hartwell, S.R., Sorlien, C.C., Dartnell, P., and Ritchie, A.C., 2017, Shelf evolution along a transpressive transform margin, Santa Barbara Channel, California: *Geosphere*, v. 13, p. 2041–2077.
- Kelsey, H.M., Engelhart, S.E., Pilarczyk, J.E., Horton, B.P., Rubin, C.M., Daryono, M.R., Ismail, N., Hawkes, A.D., Bernhardt, C.E., and Cahill, N., 2015, Accommodation space, relative sea level, and the archiving of paleo-earthquakes along subduction zones: *Geology*, v. 43, no. 8, p. 675–678, <https://doi.org/10.1130/G36706.1>.
- Khan, N.S., Horton, B.P., Engelhart, S., Rovere, A., Vacchi, M., Ashe, E.L., Törnqvist, T.E., Dutton, A., Hijma, M.P., and Shennan, I., 2019, Inception of a global atlas of sea levels since the Last Glacial Maximum: *Quaternary Science Reviews*, v. 220, p. 359–371, <https://doi.org/10.1016/j.quascirev.2019.07.016>.
- Knudsen, K.L., Witter, R.C., Garrison-Laney, C.E., Baldwin, J.N., and Carver, G.A., 2002, Past earthquake-induced rapid subsidence along the northern San Andreas fault: A paleoseismological method for investigating strike-slip faults: *Bulletin of the Seismological Society of America*, v. 92, no. 7, p. 2612–2636, <https://doi.org/10.1785/0120000613>.
- Koutsodendris, A., Brauer, A., Reed, J.M., Plessen, B., Friedrich, O., Hennrich, B., Zacharias, I., and Pross, J., 2017, Climate variability in SE Europe since 1450 AD based on a varved sediment record from Eto-liko Lagoon (Western Greece): *Quaternary Science Reviews*, v. 159, p. 63–76, <https://doi.org/10.1016/j.quascirev.2017.01.010>.
- Levy, Y., Rockwell, T.K., Shaw, J., Plesch, A., Driscoll, N., and Perea, H., 2019, Structural modeling of the Western Transverse Ranges: An imbricated thrust ramp architecture: *Lithosphere*, v. 11, no. 6, p. 868–883, <https://doi.org/10.1130/L1124.1>.
- Lienkaemper, J.J., and Bronk Ramsey, C., 2009, OxCal: Versatile tool for developing paleoearthquake chronologies—A primer: *Seismological Research Letters*, v. 80, no. 3, p. 431–434, <https://doi.org/10.1785/gssrl.80.3.431>.
- Lohmar, J.M., Macdonald, K.B., and Janes, S.A., 1980, Late Pleistocene-Holocene Sedimentary Infilling and Faunal Change in a Southern California Coastal Lagoon.
- MacDonald, K., 1969a, Molluscan faunas of Pacific coast salt marshes and tidal creeks: *The Veliger*, v. 11, no. 4, p. 399–405.
- Macdonald, K.B., 1969b, Quantitative studies of salt marsh mollusc faunas from the North American Pacific coast: *Ecological Monographs*, v. 39, no. 1, p. 33–60, <https://doi.org/10.2307/1948564>.
- Marshall, S.T., Funning, G.J., Krueger, H.E., Owen, S.E., and Loveless, J.P., 2017, Mechanical models favor a ramp geometry for the Ventura-pitas point fault, California: *Geophysical Research Letters*, v. 44, no. 3, p. 1311–1319, <https://doi.org/10.1002/2016GL072289>.

- McNeill, L.C., Goldfinger, C., Yeats, R.S., and Kulm, L.D., 1999, The effects of upper plate deformation on records of prehistoric Cascadia subduction zone earthquakes, *in* Stewart, I.S., and Vita-Finzi, C., Coastal Tectonics: Geological Society, London, Special Publication 146, no. 1, p. 321–342, <https://doi.org/10.1144/GSL.SP.1999.146.01.19>.
- Milker, Y., Horton, B.P., Vane, C.H., Engelhart, S.E., Nelson, A.R., Witter, R.C., Khan, N.S., and Bridgeland, W.T., 2015, Annual and seasonal distribution of intertidal foraminifera and stable carbon isotope geochemistry, Bandon Marsh, Oregon, USA: *Journal of Foraminiferal Research*, v. 45, no. 2, p. 146–155, <https://doi.org/10.2113/gsjfr.45.2.146>.
- Mitra, S., 2002, Fold-accommodation faults: American Association of Petroleum Geologists Bulletin, v. 86, no. 4, p. 671–693.
- Nelson, A.R., 1992, Holocene tidal-marsh stratigraphy in south-central Oregon—Evidence for localized sudden submergence in the Cascadia subduction zone.
- Nelson, A.R., Shennan, I., and Long, A.J., 1996, Identifying coseismic subsidence in tidal-wetland stratigraphic sequences at the Cascadia subduction zone of western North America: *Journal of Geophysical Research: Solid Earth*, v. 101, no. B3, p. 6115–6135, <https://doi.org/10.1029/95JB01051>.
- Nelson, A.R., Ota, Y., Umitsu, M., Kashima, K., and Matsu-shima, Y., 1998, Seismic or hydrodynamic control of rapid late-Holocene sea-level rises in southern coastal Oregon, USA?: *The Holocene*, v. 8, no. 3, p. 287–299, <https://doi.org/10.1191/095968398668600476>.
- Novoa, A., Talley, T.S., Talley, D.M., Crooks, J.A., and Reyns, N.B., 2016, Spatial and temporal examination of bivalve communities in several estuaries of Southern California and Northern Baja California, MX: *PLoS One*, v. 11, no. 2, article no. e0148220, <https://doi.org/10.1371/journal.pone.0148220>.
- Ovenshine, A., Lawson, D.E., and Bartsch-Winkler, S.R., 1976, The Placer River Silt—An intertidal deposit caused by the 1964 Alaska earthquake: *Journal of Research of the U.S. Geological Survey*, v. 4, no. 2, p. 151–162.
- Page, H.M., 1995, Variation in the natural abundance of N-15 in the halophyte, *Salicornia-Virginica*, associated with groundwater subsidies of nitrogen in a southern California salt marsh: *Oecologia*, v. 104, no. 2, p. 181–188, <https://doi.org/10.1007/BF00328583>.
- Plafker, G., 1969, Tectonics of the March 27, 1964, Alaska earthquake: U.S. Geological Survey Professional Paper 543-I, scales 1:2,000,000 and 1:500,000, 2 sheets, 74 p. text, <https://pubs.usgs.gov/pp/0543i/>.
- Pratt, T.L., Troost, K.G., Odum, J.K., and Stephenson, W.J., 2015, Kinematics of shallow backthrusts in the Seattle fault zone, Washington State: *Geosphere*, v. 11, no. 6, p. 1948–1974, <https://doi.org/10.1130/GES01179.1>.
- Reeder-Myers, L., Erlandson, J.M., Muhs, D.R., and Rick, T.C., 2015, Sea level, paleogeography, and archeology on California's Northern Channel Islands: *Quaternary Research*, v. 83, no. 2, p. 263–272, <https://doi.org/10.1016/j.yqres.2015.01.002>.
- Reimer, P.J., Austin, W.E., Bard, E., Bayliss, A., Blackwell, P.G., Ramsey, C.B., Butzin, M., Cheng, H., Edwards, R.L., and Friedrich, M., 2020, The IntCal20 Northern Hemisphere radiocarbon age calibration curve (0–55 cal kBP): *Radiocarbon*, v. 62, no. 4, p. 725–757, <https://doi.org/10.1017/RDC.2020.41>.
- Reinhardt, E.G., Nairn, R.B., and Lopez, G., 2010, Recovery estimates for the Rio Cruces after the May 1960 Chilean earthquake: *Marine Geology*, v. 269, no. 1–2, p. 18–33, <https://doi.org/10.1016/j.margeo.2009.12.003>.
- Reynolds, L.C., and Simms, A.R., 2015, Late Quaternary relative sea level in southern California and Monterey Bay: *Quaternary Science Reviews*, v. 126, p. 57–66, <https://doi.org/10.1016/j.quascirev.2015.08.003>.
- Reynolds, L.C., Simms, A.R., Ejarque, A., King, B., Anderson, R.S., Carlin, J.A., Bentz, J.M., Rockwell, T.K., and Peters, R., 2018, Coastal flooding and the 1861–2 California storm season: *Marine Geology*, v. 400, p. 49–59, <https://doi.org/10.1016/j.margeo.2018.02.005>.
- Rockwell, T.K., Clark, K., Gamble, L., Oskin, M.E., Haaker, E.C., and Kennedy, G.L., 2016, Large transverse range earthquakes cause coastal upheaval near Ventura, Southern California: *Bulletin of the Seismological Society of America*, v. 106, no. 6, p. 2706–2720, <https://doi.org/10.1785/0120150378>.
- Rodriguez-Ramirez, A., Flores-Hurtado, E., Contreras, C., Villarias-Robles, J.J.R., Jimenez-Moreno, G., Perez-Asensio, J.N., Lopez-Saez, J.A., Celestino-Perez, S., Cerrillo-Cuenca, E., and Leon, A., 2014, The role of neo-tectonics in the sedimentary infilling and geomorphological evolution of the Guadalquivir estuary (Gulf of Cadiz, SW Spain) during the Holocene: *Geomorphology*, v. 219, p. 126–140, <https://doi.org/10.1016/j.geomorph.2014.05.004>.
- Sadro, S., Gastil-Buhl, M., and Melack, J., 2007, Characterizing patterns of plant distribution in a southern California salt marsh using remotely sensed topographic and hyperspectral data and local tidal fluctuations: *Remote Sensing of Environment*, v. 110, no. 2, p. 226–239, <https://doi.org/10.1016/j.rse.2007.02.024>.
- Scott, D.B., Mudie, P.J., and Bradshaw, J.S., 2011, Coastal evolution of Southern California as interpreted from benthic foraminifera, ostracodes, and pollen: *Journal of Foraminiferal Research*, v. 41, no. 3, p. 285–307, <https://doi.org/10.2113/gsjfr.41.3.285>.
- Shennan, I., 1986, Flandrian sea-level changes in the Fensland. II: Tendencies of sea-level movement, altitudinal changes, and local and regional factors: *Journal of Quaternary Science*, v. 1, no. 2, p. 155–179, <https://doi.org/10.1002/jqs.3390010205>.
- Shennan, I., Garrett, E., and Barlow, N., 2016, Detection limits of tidal-wetland sequences to identify variable rupture modes of megathrust earthquakes: *Quaternary Science Reviews*, v. 150, p. 1–30, <https://doi.org/10.1016/j.quascirev.2016.08.003>.
- Sherrod, B.L., 2001, Evidence for earthquake-induced subsidence about 1100 yr ago in coastal marshes of southern Puget Sound, Washington: *Geological Society of America Bulletin*, v. 113, no. 10, p. 1299–1311, [https://doi.org/10.1130/0016-7606\(2001\)113<1299:EFEISA>2.0.CO;2](https://doi.org/10.1130/0016-7606(2001)113<1299:EFEISA>2.0.CO;2).
- Simms, A., Reynolds, L.C., Bentz, M., Roman, A., Rockwell, T., and Peters, R., 2016, Tectonic subsidence of California estuaries increases forecasts of relative sea-level rise: *Estuaries and Coasts*, v. 39, no. 6, p. 1571–1581, <https://doi.org/10.1007/s12237-016-0105-1>.
- Sousa, W.P., 1983, Host life history and the effect of parasitic castration on growth: A field study of *Cerithidea californica* Haldeman (Gastropoda: Prosobranchia) and its trematode parasites: *Journal of Experimental Marine Biology and Ecology*, v. 73, no. 3, p. 273–296, [https://doi.org/10.1016/0022-0981\(83\)90051-5](https://doi.org/10.1016/0022-0981(83)90051-5).
- U.S. Geological Survey (USGS), 2020, Quaternary fault and fold database for the United States. <https://usgs.maps.arcgis.com/apps/webappviewer/index.html?id=5a6038b3a1684561a9b0aadf88412fcf>.
- Tanabe, S., Nakanishi, T., Matsushima, H., and Hong, W., 2013, Sediment accumulation patterns in a tectonically subsiding incised valley: Insight from the Echigo Plain, central Japan: *Marine Geology*, v. 336, p. 33–43, <https://doi.org/10.1016/j.margeo.2012.11.006>.
- Thorne, K., MacDonald, G., Guntenspergen, G., Ambrose, R., Buffington, K., Dugger, B., Freeman, C., Janousek, C., Brown, L., and Rosencranz, J., 2018, US Pacific coastal wetland resilience and vulnerability to sea-level rise: *Science Advances*, v. 4, no. 2, article no. eaao3270, <https://doi.org/10.1126/sciadv.aao3270>.
- van de Plassche, O., 1986, *Sea-Level Research: A Manual for the Collection and Evaluation of Data*: Dordrecht, The Netherlands, Springer, 618 p., <https://doi.org/10.1007/978-94-009-4215-8>.
- Weischet, W., 1963, Further observations of geologic and geomorphic changes resulting from the catastrophic earthquake of May 1960, in Chile: *Bulletin of the Seismological Society of America*, v. 53, no. 6, p. 1237–1257, <https://doi.org/10.1785/BSSA0530061237>.
- Weltje, G.J., and Tjallingii, R., 2008, Calibration of XRF core scanners for quantitative geochemical logging of sediment cores: Theory and application: *Earth and Planetary Science Letters*, v. 274, no. 3, p. 423–438, <https://doi.org/10.1016/j.epsl.2008.07.054>.
- Wilson, R., Hemphill-Haley, E., Jaffe, B., Richmond, B., Peters, R., Graehl, N., Kelsey, H., Leeper, R., Watt, S., and McGann, M., 2014, The search for geologic evidence of distant-source tsunamis using new field data in California: Chapter C, *in* Ross, S.L., et al., *The SAFRR (Science Application for Risk Reduction) Tsunami Scenario—Improving Resilience for California*: USGS Open-File Report 2013–1170 and CGS Special Report 229, 2331–1258.
- Woodroffe, S.A., and Barlow, N.L., 2015, Reference water level and tidal datum: *in* Shennan, I., Long, A.J., and Horton, B.P., eds., *Handbook of Sea-Level Research*: Hoboken, New Jersey, USA, John Wiley & Sons, p. 171–180.
- Yokoyama, Y., Koizumi, M., Matsuzaki, H., Miyairi, Y., and Ohkouchi, N., 2010, Developing ultra-small-scale radiocarbon sample measurements at the University of Tokyo: *Radiocarbon*, v. 52, no. 2, p. 310–318.
- Yousefi, M., Milne, G.A., Love, R., and Tarasov, L., 2018, Glacial isostatic adjustment along the Pacific coast of central North America: *Quaternary Science Reviews*, v. 193, p. 288–311, <https://doi.org/10.1016/j.quascirev.2018.06.017>.

SCIENCE EDITOR: BRAD S. SINGER  
ASSOCIATE EDITOR: DAVID MACDONALD

MANUSCRIPT RECEIVED 10 JULY 2020  
REVISED MANUSCRIPT RECEIVED 1 JUNE 2021  
MANUSCRIPT ACCEPTED 17 SEPTEMBER 2021

Printed in the USA